



Satellite observations indicate substantial spatiotemporal variability in biomass burning NO_x emission factors for South America

P. Castellanos¹, K. F. Boersma^{2,3}, and G. R. van der Werf¹

¹Faculty of Earth and Life Sciences, VU University Amsterdam, the Netherlands

²Meteorology and Air Quality, Wageningen University, Wageningen, the Netherlands

³Climate Observations, Royal Netherlands Meteorological Institute, De Bilt, the Netherlands

Correspondence to: P. Castellanos (p.castellanos@vu.nl)

Received: 2 August 2013 – Published in Atmos. Chem. Phys. Discuss.: 30 August 2013

Revised: 22 January 2014 – Accepted: 24 February 2014 – Published: 17 April 2014

Abstract. Biomass burning is an important contributor to global total emissions of NO_x (NO+NO₂). Generally bottom-up fire emissions models calculate NO_x emissions by multiplying fuel consumption estimates with static biome-specific emission factors, defined in units of grams of NO per kilogram of dry matter consumed. Emission factors are a significant source of uncertainty in bottom-up fire emissions modeling because relatively few observations are available to characterize the large spatial and temporal variability of burning conditions. In this paper we use NO₂ tropospheric column observations from the Ozone Monitoring Instrument (OMI) from the year 2005 over South America to calculate monthly NO_x emission factors for four fire types: deforestation, savanna/grassland, woodland, and agricultural waste burning. In general, the spatial patterns in NO_x emission factors calculated in this work are consistent with emission factors derived from in situ measurements from the region but are more variable than published biome-specific global average emission factors widely used in bottom-up fire emissions inventories such as the Global Fire Emissions Database (GFED). Satellite-based NO_x emission factors also indicate substantial temporal variability in burning conditions. Overall, we found that deforestation fires have the lowest NO_x emission factors, on average 30 % lower than the emission factors used in GFED v3. Agricultural fire NO_x emission factors were the highest, on average a factor of 1.8 higher than GFED v3 values. For savanna, woodland, and deforestation fires, early dry season NO_x emission factors were a factor of ~1.5–2 higher than late dry season emission factors. A minimum in the NO_x emission factor seasonal cycle for deforestation fires occurred in August, the time period of severe

drought in South America in 2005, supporting the hypothesis that prolonged dry spells may lead to an increase in the contribution of smoldering combustion from large-diameter fuels, offsetting the higher combustion efficiency of dryer fine fuels. We evaluated the OMI-derived NO_x emission factors with SCIAMACHY NO₂ tropospheric column observations and found improved model performance in regions dominated by fire emissions.

1 Introduction

Human-triggered fires, both intentional and accidental, drive the spatiotemporal patterns of biomass burning in the tropics, as fire is a widely used tool to manage landscapes and clear land for new uses. Emissions from fires can control the variability and enhance the concentration of numerous trace gases (Andreae et al., 1988; Hooghiemstra et al., 2012; Langmann et al., 2009), especially in the tropics. Likewise, CO and NO_x emissions from fires comprise approximately 30 % (Arellano et al., 2006; Müller and Stavrakou, 2005) and 15 % (Jaeglé et al., 2005) of global total direct emissions, respectively. Enhanced CO and NO_x concentrations have many local and global implications such as tropospheric ozone formation and affecting the oxidizing capacity of the atmosphere by regulating the OH lifetime (Logan et al., 1981). Accurate prediction of spatial and temporal variability of fire emissions is crucial to our understanding of the Earth system as well as the impact of land use change on air quality and climate.

The approach taken to derive the Global Fire Emissions Database (GFED), a commonly used bottom-up biomass burning emissions inventory, follows Seiler and Crutzen (1980) by combining observations of burned area (Giglio et al., 2010) with a biogeochemical model (CASA: Carnegie–Ames–Stanford approach) to estimate the amount of biomass burned (van der Werf et al., 2010). These data are then partitioned into trace gas emissions using a priori emission factors, defined as the mass of a species emitted per mass of dry matter burned.

The emission factors used in GFED v3 were compiled by Andreae and Merlet (2001), who synthesized all available emission factors derived from in situ observations. Generally, emission factor measurements are grouped according to a biome class or fire use. In GFED v3, fuel consumption in each grid cell is partitioned into the following six fire types for which emission factors were selected (see Table 5 in van der Werf et al., 2010): deforestation, extratropical forest, savanna and grassland, woodland, peat, and agricultural waste burning. Thus total fire NO_x emissions in a model grid cell (E_{GFED}) are calculated by summing up the emission from all fire types (B) (Eq. 1).

$$E_{\text{GFED}} = \sum_B \text{NO}_x \text{EF}_{\text{GFED}}^B \times \text{DM}_{\text{GFED}}(B) = \begin{cases} \text{Deforestation} \\ \text{Woodland} \\ \text{Savanna} \\ \text{Agriculture} \\ \text{Forest} \\ \text{Peat} \end{cases} \quad (1)$$

In Eq. (1), $\text{NO}_x \text{EF}_{\text{GFED}}^B$ is the GFED v3 NO_x emission factor for the fire type B , and $\text{DM}_{\text{GFED}}(B)$ is the mass of dry matter consumed by the fire type B in the model grid cell. The Andreae and Merlet (2001) emission factor database is updated annually (GFED v3 emission factors include updates through 2009 (M. O. Andreae, personal communication, 2009) to include new measurements as they become available and is widely used to estimate fire trace gas emissions.

Including temporal variability in emissions factors has not been possible because of the paucity of emission factor observations. Laboratory and field experiments suggest that emission factors, even for similar vegetation types, vary significantly (Korontzi et al., 2003; Yokelson et al., 2011). As globally averaged emission factors are likely not representative of the burning conditions of individual fire events, the conversion of fuel consumption to trace gas emissions is a large source of uncertainty in bottom-up fire emission modeling (Korontzi et al., 2004; van Leeuwen and van der Werf, 2011).

Generally, NO_x emissions from biomass burning result from oxidation of fuel nitrogen, as open burns typically do not reach temperatures at which thermal NO_x can form (Urbanski et al., 2009). Other pathways for NO_x emission from biomass burning, such as the reaction of hydrocarbon radicals with atmospheric nitrogen, referred to as prompt NO_x

(Turns, 2011), are likely marginal as laboratory studies indicate the sum of emitted reactive nitrogen and N₂ account for the fuel nitrogen volatilized by burning (Kuhlbusch et al., 1991). The fraction of volatilized fuel nitrogen emitted as reactive nitrogen can vary by between 25 and 50 %. NO_x is the dominant reactive nitrogen emission during flaming combustion, while NH₃ dominates during smoldering combustion. Thus, the burning conditions and the nitrogen content of the fuel likely drive biomass burning NO_x emission factor variability (Goode et al., 2000; Yokelson et al., 2008).

McMeeking et al. (2009) reported on laboratory measurements of NO_x emission factors from burning 33 different plant species that varied from 0.04 to 9.6 g NO kg⁻¹ dry matter. When the variability in the NO_x emission factors driven by the variability in fuel nitrogen was taken into account, NO_x emission factors typically increased linearly with the modified combustion efficiency (MCE), a measure of the relative contribution of flaming and smoldering combustion to the total emissions of a fire. MCE is defined as the ratio of emitted CO₂ to CO + CO₂. At an MCE greater than 0.85–0.90, NO_x emissions typically dominate over NH₃.

In this paper we focus on biomass burning in South America, which occurs primarily over 3–4 months during the Southern Hemisphere dry season (July through October) (Giglio et al., 2006) and emits on average 15 % of total global fire emissions (van der Werf et al., 2010). Active fire observations show that the month of peak burning is September, and most of the fires occur in Brazil, although significant parts of Bolivia, Paraguay, and northern Argentina also burn. At the peak of the fire season, biomass burning NO_x emissions account for roughly 60 % of total NO_x emissions in South America (Jaeglé et al., 2005). The bulk of the emissions comes from deforestation fires along the borders of the Amazon, referred to as the arc of deforestation, which have high fuel loadings and high combustion completeness from repeated burning (Morton et al., 2008), followed by burning in the *cerrado*, a vast tropical ecoregion in the center of Brazil comprised of grasslands, savanna, and semi-deciduous forest. Fire activity and emissions have high inter-annual variability partly controlled by climate (Aragão et al., 2007; Chen et al., 2013; van der Werf et al., 2004) and also by political incentives associated with deforestation (Duncan et al., 2003; Morton et al., 2008).

Beginning in the 1980s a number of studies have documented characteristics of biomass burning in South America (Andreae et al., 1988; Crutzen et al., 1985; Ferek et al., 1998; Ward et al., 1992; Yokelson et al., 2007) (see Table 1). In the *cerrado*, fires generally burn small dry fuels and have high MCE (average: 0.94) (Ferek et al., 1998). However, the *cerrado* can range from treeless grassland to closed-canopy forest, and in many cases wood debris is a significant part of the fuel mixture. Fuel size (coarse fuels typically smolder), arrangement, and moisture content affect the MCE; thus fire intensity in woodlands is lower than in pure grasslands (burning only fine fuels) (Ward et al., 1992). Published NO_x

emission factors for savanna burning in the *cerrado* were on average 2.3 g NO kg⁻¹ dry matter (Ferek et al., 1998).

Synthesis of observations from Yucatan and African savannas indicate that early dry season savanna fires may burn higher moisture and nitrogen content fuels than late season fires (Yokelson et al., 2011). As such, early dry season savanna fires have lower MCE but higher NO_x and NH₃ emission factors than late season fires. Thus, seasonal phenology could play a large role in biomass burning NO_x emission factor variability as withered plants contain less nitrogen.

Deforestation fires primarily burn slash comprised of wood debris (including large diameter logs), foliage, the forest litter layer, and live dicot seedlings and sprouts. Occasionally, standing forest will also burn. Compared to *cerrado* fires, deforestation fires burn at lower MCE (average: 0.90) (Yokelson et al., 2008) and the smoke is from mixed-phase combustion (Ferek et al., 1998). Large wood debris is not consumed completely during a deforestation burn and can smolder for several days after the flame front passes (Kaufman et al., 1998).

Residual smoldering combustion (RSC) – generally defined as biomass consumption producing emissions not lofted by fire-induced convection – of large-diameter logs can contribute 5 % from deforestation and 40 % from pasture maintenance total emissions (Christian et al., 2007). Initial pasture maintenance fires burn partially combusted logs that remain after the deforestation burn. The larger smoldering fraction for these initial pasture maintenance fires results in a lower observed MCE and NO_x emission factor because large-diameter logs tend to burn at low MCE (~ 0.79; Christian et al., 2007). Akagi et al. (2011), who assembled a comprehensive database of globally averaged biomass burning emission factors from fresh plume measurements, list NO_x emission factors of 2.55 ± 1.44 g NO kg⁻¹ dry matter and 0.75 ± 0.59 g NO kg⁻¹ dry matter for tropical forest and pasture maintenance fires, respectively.

The contribution from RSC to total emissions has been measured by ground based sampling during several prescribed burns in Brazil. In Yokelson et al. (2007), the authors were able to sample many planned and unplanned biomass burning plumes over Brazil from an aircraft. They observed that as the dry season progressed, the MCE of lofted plumes increased, but they hypothesized that unlofted smoldering combustion emissions from coarse fuels could also increase, as prolonged dry spells will desiccate large-diameter logs.

Agricultural waste burning, particularly of sugarcane fields, is the main source of fire emissions in agricultural areas in the south of Brazil (Lara et al., 2005). Openheimer et al. (2004) observed emission factors for NO₂ of 1.3 g NO₂ kg⁻¹ dry matter for sugarcane burning in São Paulo. Taking a ratio of NO:NO₂ of 85:15 as suggested in their paper would imply a NO_x emission factor of 5.7 g NO kg⁻¹ dry matter. Measurements in the Yucatan (Yokelson et al., 2011) of agricultural waste burning indicated that the fires were predominantly flaming with NO_x

emissions factors in the range of 2.1 to 5.7 g NO kg⁻¹ dry matter.

Satellite measurements provide additional constraints on fire emission factors. Recent work has combined satellite NO₂ tropospheric column observations with satellite-based fire radiative power observations to calculate NO_x emission coefficients (units of g NO MJ⁻¹) for Californian and African savanna fires (Mebust and Cohen, 2013; Mebust et al., 2011). For African woody savanna burning they found a seasonal cycle in the observed NO_x emission coefficients with a minimum at the end of the dry season but no seasonal cycle for non-woody savannas. Their work indicates the potential for space-borne trace gas observations to better characterize biomass burning trace gas emissions, particularly for short-lived species such as NO₂, because tropospheric column concentrations are well correlated with surface emissions (Castellanos and Boersma, 2012).

In this paper we use daily NO₂ tropospheric column observations from the Ozone Monitoring Instrument (OMI) in conjunction with the Tracer Model version 5 (TM5) global chemical transport model (Huijnen et al., 2010b) to constrain total NO_x emissions from biomass burning in South America for the 2005 fire season, when widespread drought (Marengo et al., 2008) led to increased fire activity (Aragão et al., 2007) relative to the previous 5 years. We then calculated monthly NO_x emission factors for four of the fire types defined in GFED v3: deforestation, savanna/grassland, woodland, and agricultural waste burning. Key to this analysis was initial validation of the GFED v3 fuel consumption estimates with CO total column observations from the MOPITT (Measurement of Pollution in The Troposphere) instrument.

The NO_x emission factors from this work deviate substantially from the biome average emission factors currently used in GFED v3. Thus, we evaluated our spatially and temporally variable NO_x emission factor scenario with an independent data set, NO₂ tropospheric columns from the SCIAMACHY (SCanning Imaging Absorption spectroMeter for Atmospheric CHartography) instrument.

2 Satellite NO₂ observations

OMI, the Dutch–Finnish nadir-viewing imaging spectrometer aboard the EOS Aura satellite, provides measurements of backscattered radiation in the ultraviolet–visible range from 270 to 500 nm (Levelt et al., 2006). The wide field of view of the instrument allows for daily global coverage with a nominal pixel size of 13 km × 24 km at nadir, increasing to 24 km × 135 km for the largest viewing angles. The Equator-crossing time of EOS Aura is around 13:40 local time.

Table 1. Published NO_x emission factors derived from in situ measurements compared to emission factors from this work. Units are g NO kg⁻¹ dry matter. The emission factors used in GFED v3 originate from Andreae and Merlet (2001) and include updates from available measurements through 2009.

Source	Region	Deforestation			Savanna and grassland			Woodland			Agriculture waste burning			
		MCE	NO _x EF		MCE	NO _x EF		MCE	NO _x EF		MCE	NO _x EF		
Ferek et al. (1998)	Brazil	0.89	1.46 ± 0.64 ^{a,b,g}		0.94	2.3 ± 0.6 ^{a,g}								
Yokelson et al. (2008)	Brazil	0.90 ^c	1.7 ± 1.36 ^{a,g}											
Openheimer et al. (2008)	São Paolo											5.7 ^j		
Yokelson et al. (2011)	Mexico	0.92 ⁱ	4.63 ± 1.93 ^{i,g}		0.93 ⁱ	6.09 ± 0.88 ^{i,g}					0.93 ^f	3.6 ± 1.1 ^{f,g}		
Andreae and Merlet (2001)	Global		1.6 ± 0.7 ^k			3.9 ± 2.4 ^k						2.5 ± 1.0 ^k		
Andreae and Merlet + 2009 Updates (2001)	Global (GFED v3)		2.26 ^d			2.12 ^d			2.19 ^{d,e}			2.29 ^d		
Akagi et al. (2011)	Global		2.55 ± 1.4 ^g			3.9 ± 0.80 ^g						3.1 ± 1.57 ^g		
This work ^h	S. America		Jul 2.3 ± 1.2	Aug 1.4 ± 0.7	Sep 1.6 ± 0.8	Jul 2.9 ± 1.5	Aug 2.1 ± 1.1	Sep 1.8 ± 0.9	Jul 4.6 ± 2.3	Aug 2.0 ± 1.0	Sep 2.5 ± 1.2	Jul 3.4 ± 1.7	Aug 4.3 ± 2.1	Sep 4.5 ± 2.2

^aTables S1–S14_4.27.2011 in Akagi et al. (2011). ^bDerived by taking the average of tropical dry deforestation and tropical evergreen deforestation from Table S3 in Akagi et al. (2011). ^cTable 4 in Yokelson et al. (2008). ^dTable 5 in van der Werf et al. (2010). ^eDerived by taking the average of deforestation and savanna/grassland emission factor. ^fTable 2 in Yokelson et al. (2011). Emission factor at average MCE. ^gUncertainty represents the 1σ standard deviation of all measurements considered from the study. ^hEstimated uncertainty for the NO_x emission factors from this work is 50%. ⁱTables 3 and 5 in Yokelson et al. (2011). Emission factor at average MCE. Fires occurred during the early dry season. ^jCalculated assuming a NO : NO₂ ratio in emissions of 85 : 15. ^kTable 1 in Andreae and Merlet (2001).

SCIAMACHY is an eight-channel spectrometer measuring upwelling sunlight from the ultraviolet to the near infrared (240–2380 nm) in several viewing geometries (Burrows et al., 1995). SCIAMACHY is onboard the ENVISAT satellite, which has a local Equator-crossing time of 10:00. In nadir geometry the instrument performs a 32° across-track scan, equivalent to a swath width of approximately 960 km, but each observation footprint is typically 30 km × 60 km. Global coverage is achieved in 6 days. The SCIAMACHY data record ended in April 2012, when contact with the ENVISAT satellite was lost and could not be re-established.

In this work, we use OMI and SCIAMACHY NO₂ tropospheric vertical column densities from TEMIS (Tropospheric Emission Monitoring Internet Service, <http://www.temis.nl>), specifically the Dutch OMI tropospheric NO₂ (DOMINO) v2.0 (Boersma et al., 2011) and the SCIAMACHY TM4NO₂A v2.3 (Boersma et al., 2004) data products, which are produced with a common algorithm. In the retrieval, differential optical absorption spectroscopy (DOAS) is used to derive NO₂ total slant columns in the 405–465 nm and 426–451 nm wavelength range for OMI and SCIAMACHY, respectively. The stratospheric contribution to the total slant column is estimated by assimilating the measured NO₂ total slant columns in the TM4 global chemistry transport model (Dirksen et al., 2011). The stratospheric slant column is subtracted from the total column to give a tropospheric slant column. Next, tropospheric air mass factors (AMFs) are calculated with a radiative transport model given the a priori NO₂ vertical profile shape predicted by TM4, as well as the individual satellite viewing geometries, surface albedo data sets, retrieved cloud parameters, and terrain heights. Finally, tropospheric slant columns are converted to vertical columns with the AMF.

Irie et al. (2012) found the systematic bias in OMI DOMINO v2 and SCIAMACHY TM4NO₂A NO₂ tropo-

spheric columns to be less than –10 and –5 %, respectively, and statistically insignificant when comparing to MAX-DOAS observations. In Ma et al. (2013) there was a high correlation coefficient ($R = 0.91–0.93$) between DOMINO v2 columns and MAX-DOAS measurements, but a larger bias (–26 to –38 %), although 10–15 % of the bias could be explained by taking into account the spatial smoothing of the satellite pixel. The OMI and SCIAMACHY NO₂ tropospheric column data have been used extensively to study surface NO_x emissions (Ghude et al., 2013; Kaynak et al., 2009; McLinden et al., 2012).

NO₂ observations with cloud radiance fraction of greater than 50 % (cloud fraction roughly 20 %) as well as pixels affected by the row anomaly in the DOMINO data set were excluded (Braak, 2010). The selected data were re-gridded to 1° × 1° on a daily basis, where grid cell averages were taken only when the satellite had enough valid observations to cover 30 % of the grid cell.

3 Bottom-up fire emissions and the TM5 chemical transport model

We used the TM5 global chemical transport model described in detail in Huijnen et al. (2010b) to calculate the relationship between changes in NO₂ tropospheric columns and changes in fire NO_x emissions, as well as to evaluate the new NO_x emission factor scenario constrained by OMI observations. TM5 is an offline Eulerian grid model using the operator splitting technique to calculate the horizontal advection, vertical mixing, chemical transformation, and deposition of 40 chemical tracers. The ECMWF ERA-interim reanalysis fields, preprocessed to a 1° × 1° grid (Krol et al., 2005), drive meteorology in the model. The updated (Houweling et al., 1998) lumped chemical mechanism, Carbon Bond

Mechanism 4 (CBM4) (Gery et al., 1989), used in the model contains 64 gas-phase and 15 photolysis reactions. In this implementation the nitrogen oxides (NO, NO₂, NO₃, N₂O₅, HNO₄) are transported individually. Gas–aerosol partitioning of HNO₃, NH₃, NH₄⁺ to aerosol nitrate is calculated with the Equilibrium Simplified Aerosol Model (EQSAM) (Metzger et al., 2002).

We implemented the TM5 two-way nested 1° × 1° zoom function (Krol et al., 2005) within a 3° × 2° global simulation over South America (−36° S to 14° N and −84 to −30° W), where anthropogenic emissions for this region are based on the RETRO data set (Schultz et al., 2007) and biomass burning emissions are from GFED v3 at 3-hourly resolution (Mu et al., 2011). Simulations with TM5 zoomed over Europe have been compared to an ensemble of regional air quality models as well as satellite and surface in situ NO₂ observations (Huijnen et al., 2010a). The TM5 zoom falls well within the spread of the ensemble and has high spatial correlation ($r = 0.8$) with OMI observations.

Hooghiemstra et al. (2012) constrained total CO emissions at a monthly timescale with a 4D-Var inversion of MOPITT v4 thermal infrared (TIR) CO mean column concentrations for the years 2006–2010 with TM5 zoomed over South America. They found good agreement between the TM5 forward model run and satellite-observed CO column mean concentrations from April to August, and a posteriori CO total emissions were generally within 10 % of a priori emissions for these months.

To evaluate the accuracy of the GFED v3 dry matter consumption estimates over South America, we compared simulated CO concentrations to observations from MOPITT v5 (see Supplement for a description of the observations and results of the comparison in Fig. S1). CO can be considered a proxy for total dry matter consumed because CO emission factors for tropical burning are relatively constant with variability on the order of 20 % (Akagi et al., 2011; van Leeuwen et al., 2013). We find good agreement (within the 0.5×10^{18} molecules cm^{−2} accuracy of the instrument) between MOPITT v5 TIR CO total columns and our TM5 simulation in July, August, and September. This indicates that total CO emissions in South America, of which typically more than 90 % come from biomass burning (see Hooghiemstra et al., 2012), are accurate for these months. In October, however, modeled CO total columns are systematically lower than observations. It is likely that increased cloud cover at the end of the dry season introduces a low bias into the burned area observations, and consequently GFED-predicted dry matter consumption. Thus for this analysis we consider only the dry season months before October.

We take the following approach in all NO₂ model–measurements comparisons. Modeled hourly NO₂ vertical profiles are linearly interpolated to the overpass time of the observing satellite. For each model grid cell, all valid observation pixels whose pixel centers fall within the grid cell are selected. Observation-transformed modeled NO₂ tropo-

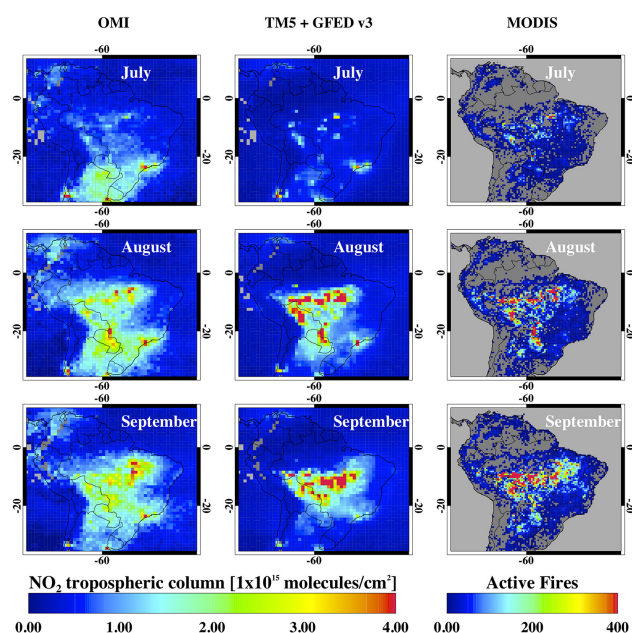


Fig. 1. Monthly average OMI-observed (left column) and modeled (middle column) NO₂ tropospheric columns. Satellite observations were re-gridded to 1° × 1° on a daily basis, where grid cell averages were taken only when the satellite had enough valid observations to fill 30 % of the grid cell. Satellite observations with cloud radiance fraction or greater than 50 % (cloud fraction roughly 20 %) were excluded. In the middle column are monthly average TM5-modeled NO₂ tropospheric columns using GFED v3 emissions, which have been transformed with the OMI averaging kernels. In the right column are MODIS Terra + Aqua cloud-corrected monthly active fires (MOD14CMH + MYD14CMH).

spheric columns are calculated with the averaging kernels (Eskes and Boersma, 2003) of each of the valid satellite pixels and the simulated trace gas vertical profile at the OMI overpass time from the grid cell. Finally, the observation-transformed columns for each grid cell are averaged together.

July through September monthly average OMI-observed and TM5-modeled NO₂ tropospheric columns as well as MODIS Terra + Aqua cloud-corrected monthly fire counts (MOD14CMH + MYD14CMH) are shown in Fig. 1. Observed and modeled NO₂ concentration enhancements correlate well spatially and temporally with observed active fires. However, in July, TM5 tends to underpredict OMI NO₂ columns, while in August and September TM5 NO₂ columns are higher than observations by more than a factor of 2 in central Brazil and Bolivia, areas where deforestation is the primary source of fire emissions. Meanwhile, in agricultural regions in the south, between São Paulo and Argentina, modeled NO₂ columns are generally lower than observations.

In a comparison of three different retrievals of GOME NO₂ tropospheric columns to 17 global chemical transport models (including TM5) using GFED v1 emissions, van Noije et al. (2006) found that the models reproduced well the

seasonal cycle of NO₂ concentrations over South America. On average, TM5-simulated NO₂ concentrations fell within the ensemble of models. Additional measurements of NO_x for South America are rare; therefore quantitative validation of model performance for this region remains elusive. However, recent model improvement and sensitivity studies give some insight into possible biases in the TM5 simulation of tropospheric NO₂. Summarizing the results of Williams et al. (2012), Mollner et al. (2010), and Stavrakou et al. (2013), which are discussed in detail in the supporting documentation, we make a conservative estimate that daytime NO₂ tropospheric columns are biased low in TM5 v3 by 0.2×10^{15} molecules cm⁻² + 0–20%. The differences between TM5 and OMI NO₂ columns, apparent in Fig. 1, exceed this estimate, indicating biases in the fire NO_x emissions.

4 NO_x emission factor calculation

Surface NO_x emissions and NO₂ tropospheric columns are closely correlated because of the short NO_x lifetime (3–10 h) in the boundary layer. Lamsal et al. (2011) proposed that fractional changes in NO₂ columns (X_{tr}) can be related to fractional changes in surface NO_x emissions (E) by a sensitivity factor β (Eq. 2).

$$\frac{\Delta E}{E} = \beta \frac{\Delta X_{tr}}{X_{tr}} \quad (2)$$

β is typically estimated with an atmospheric chemical transport model, and represents the local feedback of NO_x emissions on the NO_x lifetime and on the partitioning of NO_x into NO and NO₂. Thus with an estimate of β , one can calculate the NO_x emissions in a model grid cell (E_{OMI}) that resolve the corresponding observed NO₂ tropospheric columns with the following:

$$E_{OMI} = E_{GFED} + (E_{GFED} + E_{Background}) \times \beta \times \frac{X_{tr}^{OMI} - X_{tr}^{TM5}}{X_{tr}^{TM5}} \quad (3)$$

where E_{GFED} represents the total GFED v3 fire NO_x emitted in the grid cell during the model time step prior to the OMI overpass time, $E_{Background}$ represents the total NO_x emitted from all other biogenic and anthropogenic sources, and X_{tr}^{OMI} and X_{tr}^{TM5} are the colocated OMI-observed and TM5-simulated NO₂ tropospheric columns.

We focused our analysis on model grid cells and days where fire emissions made up more than 50 % of total emissions (the sum of anthropogenic, biogenic, and fire emissions) in the bottom-up inventory at the OMI overpass time to minimize the interference from NO_x originating from fossil fuel combustion, lightning, and microbial activity in the soil (i.e., $E_{Background}$), and the error associated with the assumption that only fire NO_x emissions account for the model-observation bias. Thus, as the majority of biomass burning in South America takes place in sparsely populated areas,

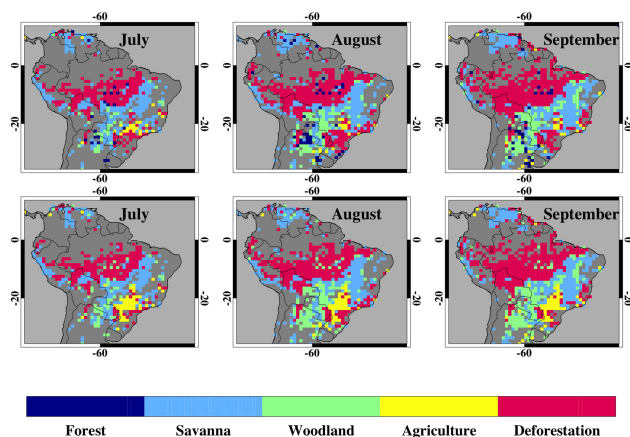


Fig. 2. In the top row are the dominant fire types according to GFED v3. Forest-fire-dominated grid cells were labeled either deforestation or woodland as described in Sect. 4. In the bottom row are the dominant fire types according to GFED v3, but with additional grid cells labeled as agriculture burning using fertilizer and manure availability greater than 60 kg ha⁻¹ (see Fig. S3) as a threshold to identify agriculture dominated grid cells.

$E_{Background}$ in Eq. (3) is marginal. Taking the alternative assumption that the ratio of fire emissions to total NO_x emissions remains constant generally has less than –5 % effect on our results, except for agricultural burning, where the range is –7 to –9 %.

We modulated the bottom-up fire NO_x emissions by 15 % and calculated the change in modeled NO₂ tropospheric columns in fire-dominated grid cells. From these NO₂ tropospheric column changes, we calculated daily β values that typically fell within the range of 0.8–1.2 (Fig. S2). The lowest values of β (<0.8) occurred in central and western Brazil as well as eastern Bolivia in August and September, where MOPITT (Fig. S1), OMI (Fig. 1), and SCIAMACHY (Fig. 5) observations indicate the highest pollution concentrations and GFED v3 estimates the highest fire emissions dominated by deforestation burning (Figs. 2 and 4). In areas where NO₂ and CO concentrations are low (e.g., the start of the fire season and eastern/southern Brazil), β is greater than 1.5, reflecting the increase in OH concentration (and decrease in NO₂ lifetime) through chemical feedbacks when NO_x emissions increase.

For each day and grid cell where there is a valid OMI observation and a corresponding monthly β , we calculate the top-down fire NO_x emissions estimate (E_{OMI}) with Eq. (3). The new NO_x emissions and the total dry matter consumption in the bottom-up inventory at the satellite overpass time were aggregated for a month according to the dominating GFED v3 fire type (deforestation, savanna/grassland, woodland, or agricultural waste burning). Each grid cell was assigned a fire type by selecting the category that contributed the most to the monthly dry matter consumption (Fig. 2). The totaled NO_x emission for a fire type was

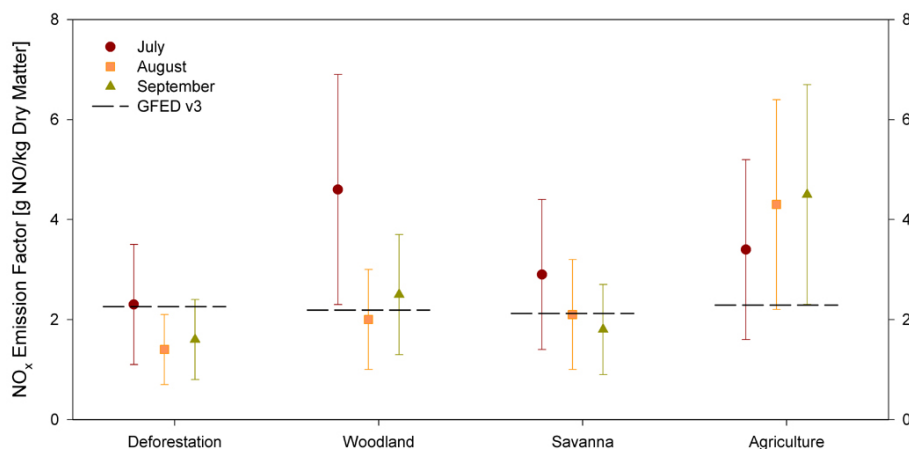


Fig. 3. Monthly NO_x emissions factors derived from daily OMI NO₂ tropospheric column observations and GFED dry matter emissions as described in Sect. 4. The numbers above each bar are the total number of daily Terra + Aqua fire counts in the grid cells that fell into the biome category in the month.

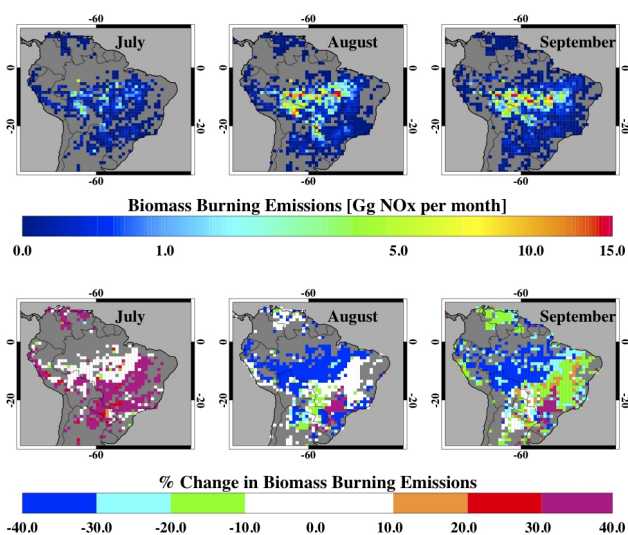


Fig. 4. Monthly fire NO_x emissions. The top row shows the GFED v3 NO_x emissions and the bottom row is the percentage change in emissions calculated by implementing the OMI-derived NO_x emission factors. Positive values reflect an increase in NO_x emissions relative to GFED v3, and negative values reflect a decrease in NO_x emissions relative to GFED v3.

divided by the corresponding dry matter consumption to give a fire-type-specific OMI-constrained NO_x emission factor ($\text{NO}_x \text{EF}_{\text{OMI}}^B$) (Eq. 4).

$$\text{NO}_x \text{EF}_{\text{OMI}}^B = \frac{\sum E_{\text{OMI}}^B}{\sum \text{DM}_{\text{GFED}}^B} B = \begin{cases} \text{Deforestation} \\ \text{Woodland} \\ \text{Savanna} \\ \text{Agriculture} \end{cases} \quad (4)$$

In Eq. (4), $\sum E_{\text{OMI}}^B$ represents the sum of OMI-constrained instantaneous fire NO_x emissions for grid cells dominated by

the fire type B . Likewise, $\sum \text{DM}_{\text{GFED}}^B$ represents the sum of GFED v3 estimated instantaneous dry matter emissions for grid cells dominated by the fire type B .

The GFED v3 partitioning of dry matter consumption into fire types assigns the deforestation label to fires in areas containing evergreen broadleaf forest also outside of the humid tropical forest domain. This classifies the grid cells in the northwest of the state of São Paulo as dominated by deforestation. However, surface observations in São Paulo (where 60 % of Brazilian sugarcane is produced) indicate agricultural waste burning, mainly pre-harvest burning of sugarcane fields, is the dominant source of pollution in São Paulo during the dry season (Oliveira et al., 2011; Openheimer et al., 2004). Thus we use the threshold of 60 kg N ha⁻¹ fertilizer and manure nitrogen availability taken from (Potter et al., 2010) as an additional mask for intensive agricultural operations to recategorize these grid cells as dominated by agricultural burning (Fig. 2). The number of agricultural burning dominated grid cells increased from 51 to 144.

Several grid cells in South America were labeled as forest fire dominated because burning occurred in forest classes outside of the humid tropical forest domain. These grid cells were few (3 % of total fire emitting grid cells in each month) and sporadic throughout the region and thus do not represent a continuous fire biome. Many forest-fire-dominated grid cells occurred within the arc of deforestation. If fuel consumption in the grid cell was almost evenly split between forest and deforestation fires (i.e., dry matter consumption for deforestation fires was at most 10 % less than forest fires), then the grid cell was labeled as deforestation dominated. Otherwise, the grid cell was assigned to the woodland category.

By summing the new NO_x emissions and dry matter consumption over a month for a fire type, we considered an ensemble of fires. This reduces the uncertainty from

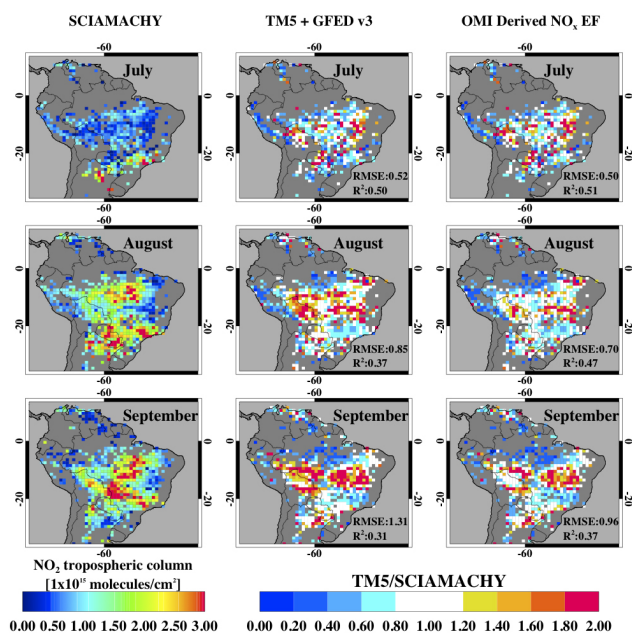


Fig. 5. Monthly average SCIAMACHY observed (left column) and the ratio of modeled to observed NO₂ tropospheric columns (center and right columns). Only grid cells that have fire emissions as indicated by GFED v3 are considered in the monthly average. Satellite observations were re-gridded to $1^\circ \times 1^\circ$ on a daily basis, where grid cell averages were taken only when the satellite had enough valid observations to fill 30 % of the grid cell. Satellite observations with cloud radiance fraction greater than 50 % (cloud fraction roughly 20 %) were excluded. In the center column are monthly average TM5 NO₂ tropospheric columns using GFED v3 emissions divided by the SCIAMACHY monthly NO₂ columns, and in the right column are the TM5 NO₂ columns using the fire NO_x emissions calculated with OMI-derived monthly NO_x emission factors divided by the SCIAMACHY monthly NO₂ columns. The modeled columns have been transformed with the SCIAMACHY averaging kernels.

partitioning the monthly fuel consumption estimates to emissions in the model time step prior to the satellite overpass time. Moreover, as we expect fires in neighboring grid cells of the same fire type to have similar fuel loads, and thus homogeneous NO_x emissions, this also reduces the errors introduced by horizontal transport, which can smear the local sensitivity of NO₂ tropospheric columns to NO_x emissions.

Thus, the primary sources of uncertainty in deriving OMI-constrained NO_x emission factors stem from the accuracy of the (1) partitioning between NO₂ and NO_y in TM5, (2) OMI NO₂ tropospheric columns, and (3) GFED v3 dry matter consumption estimates. Huijnen et al. (2010b) indicate NO_y wet deposition and NO₂ concentrations over polluted North America and Europe, where bottom-up inventories are better constrained, are generally within 30 % of observations. Boersma et al. (2011) estimated that each individual DOMINO retrieval has an uncertainty of 75 % for typical NO₂ tropospheric column concentrations of

2×10^{15} molecules cm⁻². Averaging the observations over a $1^\circ \times 1^\circ$ grid cell typically incorporates 10–30 OMI pixels, reducing the uncertainty to approximately 30 % (taking a 15 % error correlation between the observations; Miyazaki et al., 2012). In van der Werf et al. (2010), Monte Carlo simulations indicated 20 % uncertainty over continental scales for the dry matter data set. Adding errors in quadrature gives an estimated uncertainty of roughly 50 % for the NO_x emissions factors from this work, comparable to the 20–80 % variability in globally averaged NO_x emission factors derived from in situ observations (Akagi et al., 2011).

5 Results and discussion

5.1 Observation-constrained NO_x emission factors

Monthly average fire NO_x emission factors calculated from the daily adjustment of NO_x emissions to match OMI NO₂ tropospheric column observations are shown in Fig. 3 (also see Table 1). On average, we found that deforestation fires have the lowest NO_x emission factors and agricultural fires the highest, which is also the trend apparent in NO_x emission factors derived from in situ observations for the region (Table 1).

NO_x emission factors for woodland and savanna burning are comparable on average and fall in the middle of the calculated range. Our results indicate that woodland and savanna NO_x emission factors decreased from July to August by roughly 60 and 30 %, respectively. A similarly large (80 %) decrease in NO_x emission coefficient for African woody savanna burning was calculated in Mebust and Cohen (2013), although the decrease occurred over several months (the dry season is also significantly longer in Africa than in South America). Likewise, NO_x emission factors derived from in situ observations of early dry season savanna fires in the Yucatan were 80 % higher than emission factors observed for late season African savanna fires (Yokelson et al., 2011), likely due to differences in fuel nitrogen content. In the Yucatan, the average early dry season NO_x emission factor was 6.09 g NO kg⁻¹ dry matter, close to the 4.6 g NO kg⁻¹ dry matter calculated in this work for July woodland fires. The August and September OMI-derived NO_x emission factors for savanna burning (2.1 and 1.8 g NO kg⁻¹ dry matter, respectively) are comparable to the calculated woodland emission factors (2.0 and 2.5 g NO kg⁻¹ dry matter) as well as the GFED v3 global average NO_x emission factors. In GFED v3, the partitioning between savanna and woodland burning is made by determining whether herbaceous or woody fuels dominate. The distinction is likely ambiguous at $1^\circ \times 1^\circ$ resolution; thus the emission factors derived for these values may reflect a mixture of savanna and woodland burning.

The range of the deforestation emission factors (1.4–2.3 g NO kg⁻¹ dry matter) from this work falls within the

lower half of the estimates for tropical forest burning ($2.55 \pm 1.40 \text{ g NO kg}^{-1}$ dry matter) in Akagi et al. (2011). The average of the OMI-derived deforestation emission factors is 30% lower than the value used in GFED v3 ($2.26 \text{ g NO kg}^{-1}$ dry matter). Similar to savanna and woodland fires, there was a substantial (40%) decrease in deforestation NO_x emission factor from July to August. The August and September NO_x emission factor values are closer to the best-estimate deforestation emission factor (1.7 g NO kg^{-1} dry matter) from Yokelson et al. (2008) calculated with the contribution of emissions from low MCE residual smoldering combustion taken into account. This suggests that, on average, deforestation fires in August and September either had overall lower MCE, were burning higher C:N ratio fuels, or both. Thus, our findings support the hypothesis given in Yokelson et al. (2007) that under prolonged dry conditions, large-diameter fuels – which burn in the smoldering phase and have, on average, C:N ratios that are higher than leaf litter by a factor of 5 (Wang et al., 2010) – may contribute more to total fire emissions, offsetting the expected increase in MCE due to the drying out of the other fuels.

August is typically the driest month of the year in South America, and in 2005 the drought severity index (DSI) (Mu et al., 2013) indicated strong drought conditions (Fig. S4) over the region. The DSI incorporates MODIS observed normalized difference vegetation index (NDVI) and the ratio of evapotranspiration (ET) to potential evapotranspiration (PET) to determine the deviation of terrestrial water availability and plant productivity from normal levels. Thus the low deforestation NO_x emission factor and MCE in August (1.4 g NO kg^{-1} dry matter) may not be typical, but may be partly driven by the extreme drought either by desiccating the large fuel or by prompting more farmers to burn recently deforested pastures, which have a higher fraction of smoldering combustion from large-diameter logs (Christian et al., 2007). Analysis of multiple years of data is needed to confirm this.

For agricultural burning we calculated emissions factors that are on average a factor of 1.8 higher than the global average value used in GFED v3 ($2.29 \text{ g NO kg}^{-1}$ dry matter). The emission factor estimates for agriculture fires are based on only a few $1^\circ \times 1^\circ$ grid cells (4–8) that we are able to invert because we impose the limitation of considering fire dominated grid cells only. Nevertheless, our results ($3.4\text{--}4.5 \text{ g NO kg}^{-1}$ dry matter) are within the range of emission factors observed for crop residue burning in Mexico ($2.3\text{--}5.7 \text{ g NO kg}^{-1}$ dry matter) (Yokelson et al., 2011). The observations from Mexico also showed that fires in areas impacted by nitrogen deposition of urban pollution had higher NO_x emission factors than rural fires by a factor of 2. Thus, nitrogen enrichment of the biomass and litter either from fertilizer application or pollution from the São Paulo agglomeration, and high combustion completeness likely led to higher NO_x emission factors. However, because our calculations are based on few observations, and elevated background NO₂

concentrations driven by anthropogenic and biogenic emissions could bias our results, there is significant uncertainty around these values.

Recent burned area estimates suggest that total yearly emissions from small fires, mostly from agricultural burning, may be underestimated by 55% in South America in GFED v3 (Randerson et al., 2012). An underestimate in July–September agricultural fuel consumption could introduce a high bias into our calculation of emission factors for this fire type. Nevertheless, if our estimate that agricultural burning NO_x emission factors should increase by 80% is correct and yearly dry matter consumption should also be boosted by 55%, then together these results suggest that a significant source of fire NO_x emission is missing from GFED v3.

Agricultural fires are the only fire type where we calculated an increase in the NO_x emission factor from the beginning of the dry season. Because agriculture fires burn only herbaceous fuels, when drought conditions occurred in August, the fires likely burned with higher MCE.

5.2 Discussion of uncertainties and bias

In Sect. 4, we estimated that the combined uncertainty for the OMI-derived NO_x emission factors was 50%. However, biases in the simulated or observed NO₂ tropospheric columns could also affect our results. As stated in Sect. 3, we conservatively estimate that at the early afternoon overpass time of OMI, TM5 v3 NO₂ tropospheric columns are biased low by $0.2 \times 10^{15} \text{ molecules cm}^{-2} + 0\text{--}20\%$. We also estimate that a high bias in the simulated loss rate of NO₂ to OH, as well as an underestimation in the loss rate of HO₂ to aerosols, could lead to a 25% high bias in β (see Supplement). From the August and September monthly means shown in Fig. 1, it is apparent that TM5 v3 with GFED v3 emissions overestimates NO₂ tropospheric columns along the arc of deforestation, while background concentrations are underestimated. This is consistent with our findings that GFED NO_x emission factors for deforestation burning are on average too high, as well as the indications that the model NO₂ lifetime may be too short.

Model resolution and sampling errors that arise when the resolution of the NO_x emissions source is significantly smaller than the resolution of the chemistry transport model could also bias the model-predicted NO₂ concentration and NO_x lifetime. This error is most relevant for fires in July, when burning is more spatially heterogeneous and takes place when background NO₂ concentrations are low. In this case, an increase in the NO_x concentration will decrease the NO₂ lifetime. At coarse $1^\circ \times 1^\circ$ model resolution, emissions are artificially diluted, and we estimate that this could result in a 25–50% low bias in β , and a high bias in the NO₂ tropospheric column, which would offset the low bias discussed above.

In the observations, misrepresentation of the NO₂ a priori profile shape and interference from high aerosol loadings could lead to bias in the NO₂ tropospheric columns (see Supplement). If we assume that a homogeneous elevated aerosol layer develops over the region shielding the surface emissions, OMI-DOMINO v2 NO₂ tropospheric columns could be underestimated by 50 % (Lin et al., 2014). This number represents an upper limit, and is probably not representative of the typical aerosol-induced retrieval error as some aerosol correction occurs via increased cloud fractions in the DOMINO retrieval (Boersma et al., 2011).

If we incorporate these conservative bias estimates in the NO_x emission factor calculation (Eqs. 3 and 4), the “bias-corrected” OMI-derived NO_x emission factors are within 15 % of our original calculations. Given that our bias estimates are conservative, we estimate that failing to consider underlying biases in the chemical transport model and observations will contribute at most an additional 15 % uncertainty.

5.3 Evaluation of OMI-derived NO_x emission factors

We ran TM5 again with new NO_x fire emissions calculated with the OMI-constrained NO_x emission factors (NO_xEF_{OMI}^B) and compared the model results to SCIAMACHY NO₂ tropospheric columns (Figs. 4, 5, and 6). A gridded monthly field of OMI-derived NO_x emission factors was created by assigning to each grid cell the NO_xEF_{OMI}^B that corresponded with the dominant fire type. New monthly fire NO_x emissions were calculated by multiplying monthly GFED v3 dry matter consumption data with the monthly gridded OMI-derived NO_x emission factors. The emissions were rescaled to 3-hourly resolution with the GFED v3 temporal scalars (Mu et al., 2011).

Figure 4 shows a comparison of monthly NO_x emissions calculated with the OMI-constrained NO_x emission factors and GFED v3. For the region, total biomass burning NO_x emissions increased by 12 % in July, and decreased by 33 % and 26 % in August and September, respectively (Table 2). Changes in spatial variability reflect the trends in NO_x emission factors, with > 30 % increases in July for woodland and savanna fires in southern and eastern Brazil as well as in Paraguay and Argentina, but modest (±20 %) changes in August and September. NO_x emissions increased for all months in São Paulo, where agricultural burning dominates. Large decreases (20–40 %) in NO_x emissions occurred in August and September in central Brazil and in Bolivia, where there is the most fire activity and total fire emissions are largest.

In Fig. 5 we show observed monthly average NO₂ tropospheric columns for all grid cells that contained fire emissions, and the ratio between monthly average TM5 and the observations. The simulations based on OMI-derived NO_x emission factors are in better agreement with the SCIAMACHY NO₂ columns; the root-mean-square error (RMSE) decreased by 16 and 25 % in August and September, respec-

Table 2. Monthly total biomass burning NO_x emissions for South America. In the left-hand column are emissions from GFED v3, while the right-hand column shows emissions calculated by multiplying GFED v3 monthly dry matter consumption with spatially and temporally variable OMI-derived NO_x emission factors.

	GFED v3 [Gg NO]	OMI EF [Gg NO]
July	160	179
August	838	561
September	798	590
Total	1796	1330

tively, with little change in July. Figure 6 shows the probability distribution of the model bias for observed daily NO₂ concentrations over grid cells where fire emissions dominate over NO_x emissions from other sectors. In general, for all fire types the RMSE as well as the mean and standard deviation of the bias decreased, but the largest changes occurred in deforestation-dominated grid cells. Moreover, the skew towards positive bias is also reduced. That the bias is more symmetric indicates that underlying systematic errors in the simulation decreased.

Unfortunately, SCIAMACHY had only a few valid observations of agriculture burning in August. Total emissions from agriculture burning are relatively small, and SCIAMACHY overpass is earlier in the morning, while the maximum of the diurnal profile of fire emissions is early in the afternoon (close to the OMI overpass time) (Boersma et al., 2008; Mu et al., 2011). Thus, in agricultural areas of São Paulo, NO_x emissions from other sources are more likely to dominate when SCIAMACHY makes an observation. More validation is needed to constrain agricultural fires; the RMSE for these grid cells decreased by 2 %.

Deforestation emissions dominate in the grid cells with continued high bias in September despite the lower OMI-derived NO_x emission factors (Fig. 5). The high bias may result from an overestimation in the GFED v3 fire persistence approximation that is used to boost the burned area (and thus total emissions) of deforestation fires.

Although the spread in the bias decreases for all biomes, the standard deviation of the bias is still larger than the detection limit of the observations. Continued significant errors in the simulation can be expected, as other model errors will not be corrected. Moreover, our approach of binning together all fires within each biome may overrepresent fires with higher fuel consumption and therefore higher NO₂ concentrations. It is possible that smaller fires burning more herbaceous vegetation have higher NO_x emission factors, and that larger fires burning more coarse fuels have lower NO_x emission factors. A focus on resolving intra-biome variability will be the subject of future work.

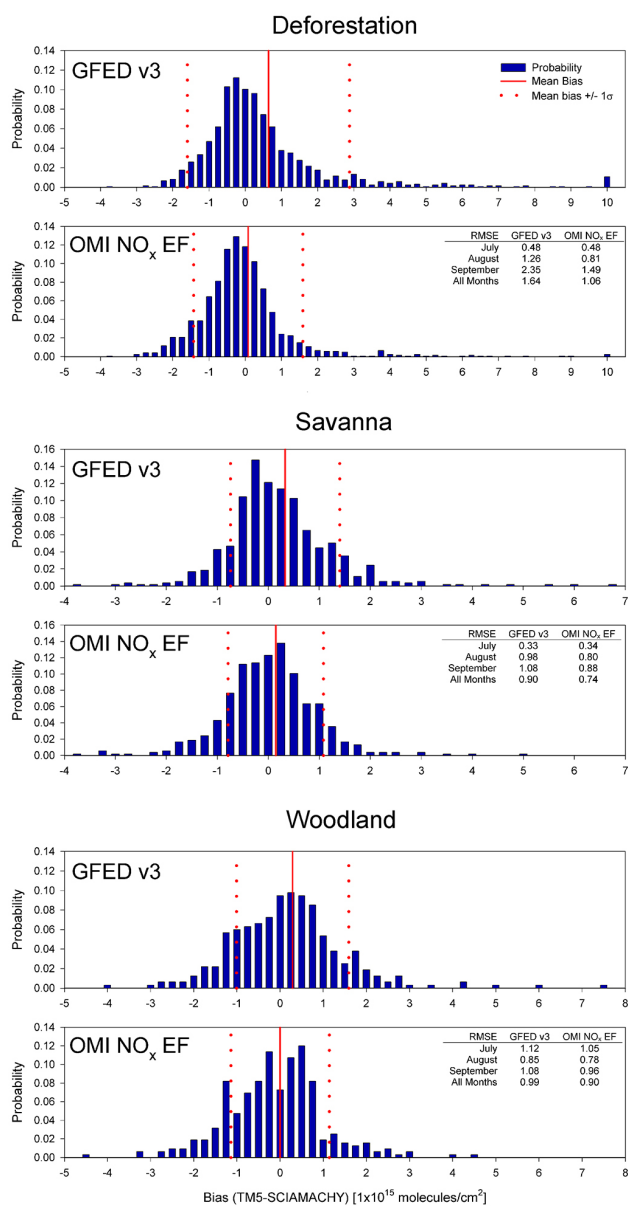


Fig. 6. The probability distribution of the bias between TM5 and SCIAMACHY daily NO₂ tropospheric columns. Only grid cells where fires contribute over 50 % to total NO_x emissions are considered.

6 Conclusions

Satellite NO₂ tropospheric column observations indicate substantial spatiotemporal variability in fire NO_x emission factors. Overall, the OMI-derived NO_x emission factors were in line with emission factors derived from in situ measurements for the region. The spatial patterns – on average highest NO_x emission factors for agricultural burning and lowest for deforestation burning – also agreed with emission factors derived from in situ measurements from the region.

For savanna and woodland burning we found the highest NO_x emission factor was in July, the start of the fire season. However, the decrease in emission factor between July and August for woodland fires was twice that of savanna fires. The trend of higher emission factors at the beginning of the dry season agrees with in situ savanna fire observations in Mexico and Africa and satellite-based NO_x emission coefficients observed over African savannas.

We found a minimum in the NO_x emission factor for deforestation burning in August that corresponded with the month of widespread severe drought in South America. Prolonged dry spells may lead to a larger contribution of smoldering combustion from large-diameter fuels to total fire emissions, which would lower the MCE and NO_x emission factor, and offset the higher MCE of the dryer, finer fuels. Thus the seasonal cycle in deforestation NO_x emission factors may have been amplified by the extreme drought conditions. Considering the combustion efficiency of the different elements of the fuel mixture could improve bottom-up modeling of fire NO_x emissions.

We also found NO_x emission factors for agricultural burning that were a factor of 1.8 higher than the global average value used in GFED v3 but were within the range of emission factors reported for crop residue burning in Mexico. However, our calculations were limited by few observations as well as uncertainties in background NO_x concentrations and agricultural fuel consumption, which increases the uncertainty for these values. Nevertheless, if our emission factor estimates are correct, then given estimates that small fires could add 55 % more yearly burned area to the current assessments in GFED v3 (Randerson et al., 2012), agricultural fire NO_x emissions may be significantly underestimated. This could have implications for simulations of local air quality, as most intensive agriculture is in close proximity to the São Paulo agglomeration, Brazil's most populous region.

We evaluated the OMI-derived NO_x emission factors with SCIAMACHY NO₂ tropospheric column observations. The model performance improved particularly for fire-dominated grid cells. The better comparison to SCIAMACHY observations and general agreement with field measurements of fire NO_x emission factors provides some confidence to our emission factor estimation approach. While the current satellite observation, chemical transport modeling, and bottom-up emissions estimates may have substantial uncertainty, which makes calculating a definitive emission factor impossible, globally averaged fire emission factors derived from in situ observations likewise have large uncertainties. The results from this work cannot close the spread in observed emission factor values; however they show that an analysis of a large number of fires aggregated over time and space yields NO_x emissions factors that are generally consistent with independent satellite observations and point observations of a few fires.

A comparison to MOPITT CO total column observations with the TM5 simulation showed that the observations were systematically underestimated at the end of the dry season, indicating there may be a low bias in burned area estimates (and therefore dry matter consumption). Increasing cloud cover leading into the wet season likely obscures burned area observations at this time.

Field campaigns that characterize the relationship between wildfire combustion efficiency and NO_x emissions, particularly targeted towards comparison to satellite NO₂ observations would be beneficial, as satellite-based NO_x emission factors may characterize burning conditions over large spatial and temporal scales. Insight into variability in combustion efficiency through NO_x could improve the estimate of other trace gases as well as particulate matter.

Supplementary material related to this article is available online at <http://www.atmos-chem-phys.net/14/3929/2014/acp-14-3929-2014-supplement.pdf>.

Acknowledgements. The authors acknowledge the MOPITT team for free use of CO observations, and funding from the Netherlands Space Office (NSO), project ALW-GO-AO/10-01. G. van der Werf acknowledges grant number 280061 from the European Research Council (ERC), and K. F. Boersma acknowledges funding by the Netherlands Organisation for Scientific Research (NWO), NWO Vidi grant 864.09.001.

Edited by: D. Spracklen

References

- Akagi, S. K., Yokelson, R. J., Wiedinmyer, C., Alvarado, M. J., Reid, J. S., Karl, T., Crounse, J. D., and Wennberg, P. O.: Emission factors for open and domestic biomass burning for use in atmospheric models, *Atmos. Chem. Phys.*, 11, 4039–4072, doi:10.5194/acp-11-4039-2011, 2011.
- Andreae, M. O. and Merlet, P.: Emission of trace gases and aerosols from biomass burning, *Global Biogeochem. Cy.*, 15, 955–966, doi:10.1029/2000GB001382, 2001.
- Andreae, M. O., Browell, E. V., Garstang, M., Gregory, G. L., Harriss, R. C., Hill, G. F., Jacob, D. J., Pereira, M. C., Sachse, G. W., Setzer, A. W., Silva Dias, P. L., Talbot, R. W., Torres, A. L., and Wofsy, S. C.: Biomass-Burning Emissions and Associated Haze Layers Over Amazonia, *J. Geophys. Res.*, 93, 1509–1527, 1988.
- Aragão, L. E. O. C., Malhi, Y., Roman-Cuesta, R. M., Saatchi, S., Anderson, L. O., and Shimabukuro, Y. E.: Spatial patterns and fire response of recent Amazonian droughts, *Geophys. Res. Lett.*, 34, L07701, doi:10.1029/2006GL028946, 2007.
- Arellano, A. F., Kasibhatla, P. S., Giglio, L., van der Werf, G. R., Randerson, J. T., and Collatz, G. J.: Time-dependent inversion estimates of global biomass-burning CO emissions using Measurement of Pollution in the Troposphere (MOPITT) measurements, *J. Geophys. Res.*, 111, D09303, doi:10.1029/2005JD006613, 2006.
- Boersma, K. F., Eskes, H. J., and Brinksma, E. J.: Error analysis for tropospheric NO₂ retrieval from space, *J. Geophys. Res.*, 109, D04311, doi:10.1029/2003JD003962, 2004.
- Boersma, K. F., Jacob, D. J., Eskes, H. J., Pinder, R. W., Wang, J., and van der A., R. J.: Intercomparison of SCIAMACHY and OMI tropospheric NO₂ columns: Observing the diurnal evolution of chemistry and emissions from space, *J. Geophys. Res.*, 113, D16S26, doi:10.1029/2007JD008816, 2008.
- Boersma, K. F., Eskes, H. J., Dirksen, R. J., van der A., R. J., Veeffkind, J. P., Stammes, P., Huijnen, V., Kleipool, Q. L., Sneep, M., Claas, J., Leitão, J., Richter, A., Zhou, Y., and Brunner, D.: An improved tropospheric NO₂ column retrieval algorithm for the Ozone Monitoring Instrument, *Atmos. Meas. Tech.*, 4, 1905–1928, doi:10.5194/amt-4-1905-2011, 2011.
- Braak, R.: Row Anomaly Flagging Rules Lookup Table, KNMI Technical Document, TN-OMIE-KNMI-950, Issue 1, <http://www.knmi.nl/omi/research/product/rowanomaly-background.php> (last access: 1 January 2013), 12 March 2010, 2010.
- Burrows, J. P., Hölzle, E., Goede, A. P. H., Visser, H., and Fricke, W.: SCIAMACHY – scanning imaging absorption spectrometer for atmospheric cartography, *Acta Astronaut.*, 35, 445–451, doi:10.1016/0094-5765(94)00278-T, 1995.
- Castellanos, P., and Boersma, K. F.: Reductions in nitrogen oxides over Europe driven by environmental policy and economic recession, *Scientific Reports*, 2, 265, doi:10.1038/srep00265, 2012.
- Chen, Y., Velicogna, I., Famiglietti, J. S., and Randerson, J. T.: Satellite observations of terrestrial water storage provide early warning information about drought and fire season severity in the Amazon, *J. Geophys. Res.-Biogeo.*, 118, 495–504, doi:10.1002/jgrg.20046, 2013.
- Christian, T. J., Yokelson, R. J., Carvalho, J. A., Griffith, D. W. T., Alvarado, E. C., Santos, J. C., Neto, T. G. S., Veras, C. A. G., and Hao, W. M.: The tropical forest and fire emissions experiment: Trace gases emitted by smoldering logs and dung from deforestation and pasture fires in Brazil, *J. Geophys. Res.*, 112, D18308, doi:10.1029/2006JD008147, 2007.
- Crutzen, P. J., Delany, A. C., Greenberg, J., Haagenson, P., Heidt, L., Lueb, R., Pollock, W., Seiler, W., Wartburg, A., and Zimmerman, P.: Tropospheric chemical composition measurements in Brazil during the dry season, *J. Atmos. Chem.*, 2, 233–256, 1985.
- Dirksen, R. J., Boersma, K. F., Eskes, H. J., Ionov, D. V., Bucsela, E. J., Levelt, P. F., and Kelder, H. M.: Evaluation of stratospheric NO₂ retrieved from the Ozone Monitoring Instrument: Intercomparison, diurnal cycle, and trending, *J. Geophys. Res.*, 116, D08305, doi:10.1029/2010JD014943, 2011.
- Duncan, B. N., Martin, R. V., Staudt, A. C., and Yevich, R.: Interannual and seasonal variability of biomass burning emissions constrained by satellite observations, *J. Geophys. Res.*, 108, 4100, doi:10.1029/2002JD002378, 2003.
- Eskes, H. J. and Boersma, K. F.: Averaging kernels for DOAS total-column satellite retrievals, *Atmos. Chem. Phys.*, 3, 1285–1291, doi:10.5194/acp-3-1285-2003, 2003.
- Ferek, R. J., Reid, J. S., Hobbs, P. V., Blake, D. R., and Liousse, C.: Emission factors of hydrocarbons, halocarbons, trace gases and particles from biomass burning in Brazil, *J. Geophys. Res.*, 103, 32107–32118, 1998.

- Gery, M. W., Whitten, G. Z., Killus, J. P., and Dodge, M. C.: A photochemical kinetics mechanism for urban and regional scale computer modeling, *J. Geophys. Res.*, 94, 12925–12956, doi:10.1029/JD094iD10p12925, 1989.
- Ghude, S. D., Pfister, G. G., Jena, C. K., van der A, R. J., Emmons, L. K., and Kumar, R.: Satellite constraints of Nitrogen Oxide (NO_x) emissions from India based on OMI observations and WRF-Chem simulations, *Geophys. Res. Lett.*, 40, doi:10.1029/2012GL053926, 2013.
- Giglio, L., Csizsar, I., and Justice, C. O.: Global distribution and seasonality of active fires as observed with the Terra and Aqua Moderate Resolution Imaging Spectroradiometer (MODIS) sensors, *J. Geophys. Res.*, 111, G02016, doi:10.1029/2005JG000142, 2006.
- Giglio, L., Randerson, J. T., van der Werf, G. R., Kasibhatla, P. S., Collatz, G. J., Morton, D. C., and DeFries, R. S.: Assessing variability and long-term trends in burned area by merging multiple satellite fire products, *Biogeosciences*, 7, 1171–1186, doi:10.5194/bg-7-1171-2010, 2010.
- Goode, J. G., Yokelson, R. J., Ward, D. E., Susott, R. A., Babbitt, R. E., Davies, M. A., and Hao, W. M.: Measurements of excess O₃, CO₂, CO, CH₄, C₂H₄, C₂H₂, HCN, NO, NH₃, HCOOH, CH₃COOH, HCHO, and CH₃OH in 1997 Alaskan biomass burning plumes by airborne Fourier transform infrared spectroscopy (AFTIR), *J. Geophys. Res.*, 105, 22147–22166, doi:10.1029/2000JD900287, 2000.
- Hooghiemstra, P. B., Krol, M. C., Leeuwen, T. T., van der Werf, G. R., Novelli, P. C., Deeter, M. N., Aben, I., and Röckmann, T.: Interannual variability of carbon monoxide emission estimates over South America from 2006 to 2010, *J. Geophys. Res.*, 117, D15308, doi:10.1029/2012JD017758, 2012.
- Houweling, S., Dentener, F., and Lelieveld, J.: The impact of non-methane hydrocarbon compounds on tropospheric photochemistry, *J. Geophys. Res.*, 103, 10673–10696, 1998.
- Huijnen, V., Eskes, H. J., Poupkou, A., Elbern, H., Boersma, K. F., Foret, G., Sofiev, M., Valdebenito, A., Flemming, J., Stein, O., Gross, A., Robertson, L., D'Isidoro, M., Kioutsioukis, I., Friese, E., Amstrup, B., Bergstrom, R., Strunk, A., Vira, J., Zyryanov, D., Maurizi, A., Melas, D., Peuch, V.-H., and Zerefos, C.: Comparison of OMI NO₂ tropospheric columns with an ensemble of global and European regional air quality models, *Atmos. Chem. Phys.*, 10, 3273–3296, doi:10.5194/acp-10-3273-2010, 2010a.
- Huijnen, V., Williams, J., van Weele, M., van Noije, T., Krol, M., Dentener, F., Segers, A., Houweling, S., Peters, W., de Laat, J., Boersma, F., Bergamaschi, P., van Velthoven, P., Le Sager, P., Eskes, H., Alkemade, F., Scheele, R., Nédélec, P., and Pätz, H.-W.: The global chemistry transport model TM5: description and evaluation of the tropospheric chemistry version 3.0, *Geosci. Model Dev.*, 3, 445–473, doi:10.5194/gmd-3-445-2010, 2010b.
- Irie, H., Boersma, K. F., Kanaya, Y., Takashima, H., Pan, X., and Wang, Z. F.: Quantitative bias estimates for tropospheric NO₂ columns retrieved from SCIAMACHY, OMI, and GOME-2 using a common standard for East Asia, *Atmos. Meas. Tech.*, 5, 2403–2411, doi:10.5194/amt-5-2403-2012, 2012.
- Jaeglé, L., Steinberger, L., Martin, R. V., and Chance, K.: Global partitioning of NO_x sources using satellite observations: Relative roles of fossil fuel combustion, biomass burning and soil emissions, *Faraday Discuss.*, 130, 407–423, doi:10.1039/B502128F, 2005.
- Kaufman, Y. J., Hobbs, P. V., Kirchoff, W. J. H., Artaxo, P., Rember, L. A., Holben, B. N., King, M. D., Ward, D. E., Prins, E. M., Longo, K. M., Mattos, L. F., Nobre, C. A., Spinhirne, J. D., Ji, Q., Thompson, A. M., Gleason, J. F., Christopher, S. A., and Tsay, S. C.: Smoke, Clouds, and Radiation-Brazil (SCAR-B) experiment, *J. Geophys. Res.*, 103, 31783–31808, doi:10.1029/98JD02281, 1998.
- Kaynak, B., Hu, Y., Martin, R. V., Sioris, C. E., and Russell, A. G.: Comparison of weekly cycle of NO₂ satellite retrievals and NO_x emission inventories for the continental United States, *J. Geophys. Res.*, 114, D05302, doi:10.1029/2008JD010714, 2009.
- Korontzi, S., Ward, D. E., Susott, R. A., Yokelson, R. J., Justice, C. O., Hobbs, P. V., Smithwick, E. A. H., and Hao, W. M.: Seasonal variation and ecosystem dependence of emission factors for selected trace gases and PM_{2.5} for southern African savanna fires, *J. Geophys. Res.*, 108, 4758, doi:10.1029/2003JD003730, 2003.
- Korontzi, S., Roy, D. P., Justice, C. O., and Ward, D. E.: Modeling and sensitivity analysis of fire emissions in southern Africa during SAFARI 2000, *Remote Sens. Environ.*, 92, 255–275, doi:10.1016/j.rse.2004.06.010, 2004.
- Krol, M., Houweling, S., Bregman, B., van den Broek, M., Segers, A., van Velthoven, P., Peters, W., Dentener, F., and Bergamaschi, P.: The two-way nested global chemistry-transport zoom model TM5: algorithm and applications, *Atmos. Chem. Phys.*, 5, 417–432, doi:10.5194/acp-5-417-2005, 2005.
- Kuhlbusch, T. A., Lobert, J. M., Crutzen, P. J., and Warneck, P.: Molecular nitrogen emissions from denitrification during biomass burning, *Nature*, 351, 135–137, doi:10.1038/351135a0, 1991.
- Lamsal, L. N., Martin, R. V., Padmanabhan, A., Donkelaar, A. V., Zhang, Q., Sioris, C. E., Chance, K., Kurosu, T. P., and Newchurch, M. J.: Application of satellite observations for timely updates to global anthropogenic NO_x emission inventories, *Geophys. Res. Lett.*, 38, L05810, doi:10.1029/2010GL046476, 2011.
- Langmann, B., Duncan, B., Textor, C., Trentmann, J., and van der Werf, G. R.: Vegetation fire emissions and their impact on air pollution and climate, *Atmos. Environ.*, 43, 107–116, doi:10.1016/j.atmosenv.2008.09.047, 2009.
- Lara, L. L., Artaxo, P., Martinelli, L. A., Camargo, P. B., Victoria, R. L., and Ferraz, E. S. B.: Properties of aerosols from sugar-cane burning emissions in Southeastern Brazil, *Atmos. Environ.*, 39, 4627–4637, doi:10.1016/j.atmosenv.2005.04.026, 2005.
- Levelt, P. F., van den Oord, G. H. J., Dobber, M. R., Malkki, A., Huib Visser, Johan de Vries, Stammes, P., Lundell, J. O. V., and Saari, H.: The ozone monitoring instrument, *IEEE T. Geosci. Remote*, 44, 1093–1101, doi:10.1109/TGRS.2006.872333, 2006.
- Lin, J.-T., Martin, R. V., Boersma, K. F., Sneep, M., Stammes, P., Spurr, R., Wang, P., Van Roozendael, M., Clémer, K., and Irie, H.: Retrieving tropospheric nitrogen dioxide from the Ozone Monitoring Instrument: effects of aerosols, surface reflectance anisotropy, and vertical profile of nitrogen dioxide, *Atmos. Chem. Phys.*, 14, 1441–1461, doi:10.5194/acp-14-1441-2014, 2014.
- Logan, J. A., Prather, M. J., Wofsy, S. C., and McElroy, M. B.: Tropospheric chemistry: A global perspective, *J. Geophys. Res.*, 86, 7210–7254, doi:10.1029/JC086iC08p07210, 1981.
- Ma, J. Z., Beirle, S., Jin, J. L., Shaiganfar, R., Yan, P., and Wagner, T.: Tropospheric NO₂ vertical column densities over Beijing: re-

- sults of the first three years of ground-based MAX-DOAS measurements (2008–2011) and satellite validation, *Atmos. Chem. Phys.*, 13, 1547–1567, doi:10.5194/acp-13-1547-2013, 2013.
- Marengo, J. A., Nobre, C. A., Tomasella, J., Oyama, M. D., Sampaio de Oliveira, G., de Oliveira, R., Camargo, H., Alves, L. M., and Brown, I. F.: The Drought of Amazonia in 2005, *J. Climate*, 21, 495–516, doi:10.1175/2007JCLI1600.1, 2008.
- McLinden, C. A., Fioletov, V., Boersma, K. F., Krotkov, N., Sioris, C. E., Veefkind, J. P., and Yang, K.: Air quality over the Canadian oil sands: A first assessment using satellite observations, *Geophys. Res. Lett.*, 39, L04804, doi:10.1029/2011GL050273, 2012.
- McMeeking, G. R., Kreidenweis, S. M., Baker, S., Carrico, C. M., Chow, J. C., Collett Jr., J. L., Hao, W. M., Holden, A. S., Kirchstetter, T. W., Malm, W. C., Moosmüller, H., Sullivan, A. P., and Wold, C. E.: Emissions of trace gases and aerosols during the open combustion of biomass in the laboratory, *J. Geophys. Res.*, 114, D19210, doi:10.1029/2009JD011836, 2009.
- Mebust, A. K. and Cohen, R. C.: Observations of a seasonal cycle in NO_x emissions from fires in African woody savannas, *Geophys. Res. Lett.*, 40, 1451–1455, doi:10.1002/grl.50343, 2013.
- Mebust, A. K., Russell, A. R., Hudman, R. C., Valin, L. C., and Cohen, R. C.: Characterization of wildfire NO_x emissions using MODIS fire radiative power and OMI tropospheric NO₂ columns, *Atmos. Chem. Phys.*, 11, 5839–5851, doi:10.5194/acp-11-5839-2011, 2011.
- Metzger, S., Dentener, F., Pandis, S. N., and Lelieveld, J.: Gas/aerosol partitioning: 1. A computationally efficient model, *J. Geophys. Res.*, 107, 4312, doi:10.1029/2001JD001102, 2002.
- Miyazaki, K., Eskes, H. J., and Sudo, K.: Global NO_x emission estimates derived from an assimilation of OMI tropospheric NO₂ columns, *Atmos. Chem. Phys.*, 12, 2263–2288, doi:10.5194/acp-12-2263-2012, 2012.
- Mollner, A. K., Valluvadasan, S., Feng, L., Sprague, M. K., Okumura, M., Milligan, D. B., Bloss, W. J., Sander, S. P., Martien, P. T., Harley, R. A., McCoy, A. B., and Carter, W. P. L.: Rate of Gas Phase Association of Hydroxyl Radical and Nitrogen Dioxide, *Science*, 330, 646–649, doi:10.1126/science.1193030, 2010.
- Morton, D. C., DeFries, R. S., Randerson, J. T., Giglio, L., SCHROEDER, W., and van der Werf, G. R.: Agricultural intensification increases deforestation fire activity in Amazonia, *Global Chang. Biol.*, 14, 2262–2275, doi:10.1111/j.1365-2486.2008.01652.x, 2008.
- Mu, M., Randerson, J. T., van der Werf, G. R., Giglio, L., Kasibhatla, P., Morton, D., Collatz, G. J., DeFries, R. S., Hyer, E. J., Prins, E. M., Griffith, D. W. T., Wunch, D., Toon, G. C., Sherlock, V., and Wennberg, P. O.: Daily and 3-hourly variability in global fire emissions and consequences for atmospheric model predictions of carbon monoxide, *J. Geophys. Res.*, 116, D24303, doi:10.1029/2011JD016245, 2011.
- Mu, Q., Zhao, M., Kimball, J. S., McDowell, N. G., and Running, S. W.: A remotely sensed global terrestrial drought severity index, *B. Am. Meteorol. Soc.*, 94, 83–98, 2013.
- Müller, J.-F. and Stavrou, T.: Inversion of CO and NO_x emissions using the adjoint of the IMAGES model, *Atmos. Chem. Phys.*, 5, 1157–1186, doi:10.5194/acp-5-1157-2005, 2005.
- Oliveira, P. L., de Figueiredo, B. R., and Cardoso, A. A.: Atmospheric pollutants in São Paulo state, Brazil and effects on human health – a review, *Geochimica Brasiliensis*, 25, 17–24, 2011.
- Openheimer, C., Tsanev, V. I., Allen, A. G., McGonigle, A. J. S., Cardoso, A. A., Wiatr, A., Paterlini, W., and de Mello Dias, C.: NO₂ Emissions from Agricultural Burning in São Paulo, Brazil, *Environ. Sci. Technol.*, 38, 4557–4561, doi:10.1021/es0496219, 2004.
- Potter, P., Ramankutty, N., Bennett, E. M., and Donner, S. D.: Characterizing the Spatial Patterns of Global Fertilizer Application and Manure Production, *Earth Interact.*, 14, 1–22, doi:10.1175/2009EI288.1, 2010.
- Randerson, J. T., Chen, Y., Werf, G. R., Rogers, B. M., and Morton, D.: Global burned area and biomass burning emissions from small fires, *J. Geophys. Res.*, 117, G04012, doi:10.1029/2012JG002128, 2012.
- Schultz, M. G., Backman, L., Balkanski, Y., Bjoerndalsaeter, S., Brand, R., Burrow, J. P., Dalsoeren, S., de Vasconcelos, M., Grodtmann, B., Jauglustaine, D. A., Heil, A., Hoelzemann, J. J., Isaksen, I. S. A., Kaurola, J., Knor, W., Kadstaetter-Weibenmayer, A., Mota, B., Oom, D., Pacyna, J., Panasiuk, D., Pereira, J. M. C., Pulles, T., Pyle, J., Rast, S., Richter, A., Savage, N., Schnadt, C., Spessa, A., Staehelin, J., Sundet, J. K., Szopa, S., van het Bolscher, M., van Noije, T. P. C., van Velthoven, P., Thonicke, K., Vik, A. F., and Wittrock, F.: Reanalysis of the tropospheric chemical composition over the past 40 years: Final Report, edited by: Schultz, M. G., Max Planck Institute for Meteorology, Jülich/Hamburg, 2007.
- Seiler, W. and Crutzen, P. J.: Estimates of gross and net fluxes of carbon between the biosphere and the atmosphere from biomass burning, *Climate Change*, 2, 207–247, doi:10.1007%2FBF00137988, 1980.
- Stavrou, T., Müller, J.-F., Boersma, K. F., van der A, R. J., Kurokawa, J., Ohara, T., and Zhang, Q.: Key chemical NO_x sink uncertainties and how they influence top-down emissions of nitrogen oxides, *Atmos. Chem. Phys.*, 13, 9057–9082, doi:10.5194/acp-13-9057-2013, 2013.
- Turns, S.: An introduction to combustion concepts and applications, 3rd Edn., McGraw-Hill, New York, 732 pp., 2012.
- Urbanski, S. P., Hao, W. M., and Baker, S.: Chemical Composition of Wildland Fire Emissions, in: *Developments in Environmental Science*, vol. 8, 79–107, Elsevier B. V., 2009.
- van der Werf, G. R., Randerson, J. T., Collatz, G. J., Giglio, L., Kasibhatla, P., Arellano, A. F., Olsen, S. C., and Kasischke, E. S.: Continental-Scale Partitioning of Fire Emissions During the 1997 to 2001 El Niño/La Niña Period, *Science*, 303, 73–76, doi:10.1126/science.1090753, 2004.
- van der Werf, G. R., Randerson, J. T., Giglio, L., Collatz, G. J., Mu, M., Kasibhatla, P. S., Morton, D. C., DeFries, R. S., Jin, Y., and van Leeuwen, T. T.: Global fire emissions and the contribution of deforestation, savanna, forest, agricultural, and peat fires (1997–2009), *Atmos. Chem. Phys.*, 10, 11707–11735, doi:10.5194/acp-10-11707-2010, 2010.
- van Leeuwen, T. T. and van der Werf, G. R.: Spatial and temporal variability in the ratio of trace gases emitted from biomass burning, *Atmos. Chem. Phys.*, 11, 3611–3629, doi:10.5194/acp-11-3611-2011, 2011.
- van Leeuwen, T. T., Peters, W., Krol, M. C., and van der Werf, G. R.: Dynamic biomass burning emission factors and their impact on atmospheric CO mixing ratios, *J. Geophys. Res.*, 118, 6797–6815, doi:10.1002/jgrd.50478, 2013.

- van Noije, T. P. C., Eskes, H. J., Dentener, F. J., Stevenson, D. S., Ellingsen, K., Schultz, M. G., Wild, O., Amann, M., Atherton, C. S., Bergmann, D. J., Bey, I., Boersma, K. F., Butler, T., Co-fala, J., Drevet, J., Fiore, A. M., Gauss, M., Hauglustaine, D. A., Horowitz, L. W., Isaksen, I. S. A., Krol, M. C., Lamarque, J.-F., Lawrence, M. G., Martin, R. V., Montanaro, V., Müller, J.-F., Pitari, G., Prather, M. J., Pyle, J. A., Richter, A., Rodriguez, J. M., Savage, N. H., Strahan, S. E., Sudo, K., Szopa, S., and van Roozendaal, M.: Multi-model ensemble simulations of tropospheric NO₂ compared with GOME retrievals for the year 2000, *Atmos. Chem. Phys.*, 6, 2943–2979, doi:10.5194/acp-6-2943-2006, 2006.
- Wang, Y. P., Law, R. M., and Pak, B.: A global model of carbon, nitrogen and phosphorus cycles for the terrestrial biosphere, *Biogeosciences*, 7, 2261–2282, doi:10.5194/bg-7-2261-2010, 2010.
- Ward, D. E., Susott, R. A., Kauffman, R. E., Babbitt, R. E., Cummings, D. L., Dias, B., Holben, B. N., Kaufman, Y. J., Rasmussen, R. A., and Setzer, A. W.: Smoke and fire characteristics for cerrado and deforestation burns in Brazil: BASE-B experiment, *J. Geophys. Res.*, 97, 14601–14619, 1992.
- Williams, J. E., Strunk, A., Huijnen, V., and van Weele, M.: The application of the Modified Band Approach for the calculation of on-line photodissociation rate constants in TM5: implications for oxidative capacity, *Geosci. Model Dev.*, 5, 15–35, doi:10.5194/gmd-5-15-2012, 2012.
- Yokelson, R. J., Karl, T., Artaxo, P., Blake, D. R., Christian, T. J., Griffith, D. W. T., Guenther, A., and Hao, W. M.: The Tropical Forest and Fire Emissions Experiment: overview and airborne fire emission factor measurements, *Atmos. Chem. Phys.*, 7, 5175–5196, doi:10.5194/acp-7-5175-2007, 2007.
- Yokelson, R. J., Christian, T. J., Karl, T. G., and Guenther, A.: The tropical forest and fire emissions experiment: laboratory fire measurements and synthesis of campaign data, *Atmos. Chem. Phys.*, 8, 3509–3527, doi:10.5194/acp-8-3509-2008, 2008.
- Yokelson, R. J., Burling, I. R., Urbanski, S. P., Atlas, E. L., Adachi, K., Buseck, P. R., Wiedinmyer, C., Akagi, S. K., Toohey, D. W., and Wold, C. E.: Trace gas and particle emissions from open biomass burning in Mexico, *Atmos. Chem. Phys.*, 11, 6787–6808, doi:10.5194/acp-11-6787-2011, 2011.